



# Contiguous polarisation spectra of the Earth from 300 to 850 nm measured by GOME-2 onboard MetOp-A

L. G. Tilstra<sup>1</sup>, R. Lang<sup>2</sup>, R. Munro<sup>2</sup>, I. Aben<sup>3</sup>, and P. Stammes<sup>1</sup>

<sup>1</sup>Royal Netherlands Meteorological Institute (KNMI), De Bilt, the Netherlands

<sup>2</sup>European Organisation for the Exploitation of Meteorological Satellites (EUMETSAT), Darmstadt, Germany

<sup>3</sup>SRON Netherlands Institute for Space Research, Utrecht, the Netherlands

Correspondence to: L. G. Tilstra (tilstra@knmi.nl) and P. Stammes (stammes@knmi.nl)

Received: 23 October 2013 – Published in Atmos. Meas. Tech. Discuss.: 19 December 2013

Revised: 31 March 2014 – Accepted: 3 June 2014 – Published: 9 July 2014

**Abstract.** In this paper we present the first contiguous high-resolution spectra of the Earth's polarisation observed by a satellite instrument. The measurements of the Stokes fraction  $Q/I$  are performed by the spectrometer GOME-2 onboard the MetOp-A satellite. Polarisation measurements by GOME-2 are performed by onboard polarisation measurement devices (PMDs) and the high-resolution measurements discussed in this paper are taken in the special “PMD RAW” mode of operation. The spectral resolution of these PMD RAW polarisation measurements varies from 3 nm in the ultraviolet (UV) to 35 nm in the near-infrared wavelength range. We first compare measurements of the polarisation from cloud-free scenes with radiative transfer calculations for a number of cases. We find good agreement but also a spectral discrepancy at 800 nm, which we attribute to remaining imperfections in the calibration key data. Secondly, we study the polarisation of scenes with special scattering geometries that normally lead to near-zero  $Q/I$ . The GOME-2 polarisation spectra indeed show this behaviour and confirm the existence of the small discrepancy found earlier. Thirdly, we study the Earth polarisation for a variety of scenes. This provides a blueprint of  $Q/I$  over land and sea surfaces for various degrees of cloud cover. Fourthly, we compare the spectral dependence of measurements of  $Q/I$  in the UV with the generalised distribution function proposed by Schutgens and Stammes (2002) to describe the shape of the UV polarisation spectrum. The GOME-2 data confirm that these functions match the spectral behaviour captured by the GOME-2 PMD RAW mode.

## 1 Introduction

Measurements of the atmospheric state of polarisation form an important addition to knowledge of the intensity of the backscattered sunlight as it completes the description of the top of atmosphere (TOA) signal and (therefore) enables a more accurate retrieval of atmospheric properties and constituents (Mishchenko and Travis, 1997). A good example of this is the retrieval of aerosol properties over land made possible by measurements of polarisation performed by the POLDER (Deschamps et al., 1994) instruments (Deuzé et al., 2001; Hasekamp and Landgraf, 2007; Tanré et al., 2011). The POLDER instruments were designed to measure the state of polarisation for the purpose of improving retrieval possibilities.

There are also instruments that measure the state of polarisation primarily for the purpose of improving their radiometric calibration. Examples are GOME (Burrows et al., 1999), SCIAMACHY (Bovensmann et al., 1999), and the GOME-2 instruments (Callies et al., 2000) onboard the MetOp range of satellites. The spectral detectors of these instruments, which are responsible for the detection of the Earth radiances, are not only sensitive to the intensity of the detected light, but also to its polarisation. Knowledge of the state of polarisation is therefore required to be able to perform a correction for the polarisation sensitivity (Schutgens and Stammes, 2003; Lichtenberg et al., 2006; Munro and Lang, 2011).

Essential for both purposes is (good knowledge of) the quality of the polarisation measurements. Validation of atmospheric polarisation measurements is generally speaking more challenging than validation of Earth reflectance

measurements. For instance, satellite intercomparisons between the small fleet of polarisation-measuring satellite instruments are complicated or even impossible because of the strong dependence of the state of polarisation on the scattering geometry. A reliable intercomparison would require the instruments to record the same footprint at approximately the same time with more or less identical viewing and solar geometries (as in e.g. Tilstra and Stammes, 2007). Another method used for polarisation validation is based on analysing the polarisation for (the few) special geometries along the orbit for which the state of polarisation can be predicted (Aben et al., 2003). Strictly speaking, this only validates the atmospheric polarisation measurements for these special geometries. Other methods of validation rely on simulations based on radiative transfer calculations or employing alternative approaches of polarisation retrieval (Tilstra and Stammes, 2005).

This paper focuses on the polarisation measurements of the GOME-2 instrument. More specifically, it focuses on its so-called “PMD RAW” mode, which is a special mode in which the entire, contiguous spectrum of polarisation is measured from 300 to 850 nm with a high to moderate spectral resolution between 3 and 35 nm. Contiguous spectra of atmospheric polarisation have been measured before over the (UV-)VIS-NIR wavelength range with high spectral resolution (Aben et al., 1999; Boesche et al., 2006). However, these measurements of the scattered skylight were performed using ground-based instruments. All of the satellite instruments that were mentioned earlier in this section perform their polarisation measurements for specific wavelength bands in the spectrum. Other remote-sensing spectrometers exist that do measure contiguous polarisation spectra, such as the GOSAT instrument (Kuze et al., 2009), but only in specific small wavelength windows. The GOME-2 instrument in its PMD RAW mode is the first instrument that observes the Earth polarisation at the TOA over the entire UV-VIS-NIR wavelength range.

The goal of this paper is twofold. First, to introduce the measurements of polarisation spectra taken by GOME-2 and to validate the quality of the polarisation spectra. Validation of the spectra is not only relevant to applications making use of the measured spectra. It is also a check of the calibration of the normal polarisation measurements, as the radiometric calibration data used for the normal polarisation measurements has been partly derived from PMD RAW measurements (Lang, 2010). Secondly, we want to present the first measured contiguous polarisation spectra taken from the TOA and present (measured) blueprints of atmospheric polarisation for typical Earth scenes under typical circumstances.

The outline of this paper is as follows. In Sect. 2 we start off with a short introduction of atmospheric polarisation in terms of Stokes fractions. Section 3 briefly introduces the GOME-2 satellite instrument, and describes how the PMD RAW polarisation measurements are performed. Sections 4

and 5 both present the results of validation studies. The validation in Sect. 4 is based on comparisons with model simulations. The validation in Sect. 5 is based on the use of special geometries along the orbit for which the Stokes fraction  $Q/I$  is close to zero irrespective of the underlying scene characteristics. In Sect. 6 we present high-resolution polarisation spectra of Stokes fraction  $Q/I$  for a range of typical Earth scenes. In Sect. 7 we use the high-resolution spectral measurements in the UV wavelength range to confirm that the spectrum of Stokes fraction  $Q/I$  can be described well in the UV by a generalised distribution function (GDF). The paper ends with a summary and conclusions.

## 2 Definitions

The amount of circularly polarised light reflected by the Earth’s atmosphere is negligible (Coulson, 1988), and therefore only linearly polarised light needs to be considered in the current context. Linearly polarised light can be described by the Stokes parameters  $\{I, Q, U\}$ . These three parameters are defined as follows (van de Hulst, 1981; Hovenier et al., 2004):

$$I = I_{\parallel} + I_{\perp} = I_{0^{\circ}} + I_{90^{\circ}}, \quad (1)$$

$$Q = I_{\parallel} - I_{\perp} = I_{0^{\circ}} - I_{90^{\circ}}, \quad (2)$$

$$U = I_{45^{\circ}} - I_{135^{\circ}}, \quad (3)$$

where  $I$  is the total intensity of the light and  $Q$  and  $U$  together contain all the information about the linear polarisation. In Eqs. (1)–(3) the angles denote the direction of the transmission axis of a linear polariser, relative to some reference plane. In this paper, and for GOME-2, this reference plane is the local meridian plane, defined as the plane containing the local zenith and the spectrometer’s viewing direction. The Stokes parameters  $Q$  and  $U$  can also be expressed in terms of the degree of linear polarisation  $P$  and the direction of linear polarisation  $\chi$  (van de Hulst, 1981):

$$Q/I = P \cos 2\chi \quad (4)$$

$$U/I = P \sin 2\chi. \quad (5)$$

In this representation, the degree of linear polarisation  $P$  and the direction of linear polarisation  $\chi$  are defined as

$$P = \sqrt{Q^2 + U^2}/I; \quad \tan 2\chi = U/Q. \quad (6)$$

The normalised quantities  $Q/I$  and  $U/I$  are referred to as Stokes *fractions*. The direction of linear polarisation  $\chi$  is mainly determined by the geometry that defines the sun-atmosphere-satellite system. A study has shown that it deviates very little from its theoretical single scattering value (Schutgens et al., 2004). This means that we can use  $\chi \approx \chi_{ss}$  in good approximation, where  $\chi_{ss}$  is calculated from geometry only. As for the degree of linear polarisation  $P$ , in general it not only depends on the scattering geometry, but also

on the properties of the observed scene. Inside strong gaseous absorption bands, e.g. below  $\sim 300$  nm, where ozone absorption is so strong that single scattering is a good approximation, the degree of polarisation does only depend on the scattering geometry, and is given by (e.g. Chandrasekhar, 1960; Schutgens and Stammes, 2002)

$$P_{ss} = \frac{1 - \cos^2 \Theta}{1 + \Delta + \cos^2 \Theta}, \quad (7)$$

where  $\Theta$  is the single scattering angle, and  $\Delta = 2\rho_n/(1 - \rho_n)$  is a correction factor for depolarisation due to molecular anisotropy. The parameter  $\rho_n$  is the depolarisation factor for natural light which may be calculated directly (van de Hulst, 1981) from the reported values of the King correction factor  $F_K$  found in, for instance, Bates (1984). At 300 nm,  $F_K = 1.055$  leading to  $\rho_n = 0.03178$ . The correction factor  $\Delta$  thus amounts to 0.0656 at this wavelength.

In this paper, the Earth's reflectance is defined as

$$R = \frac{\pi I}{\mu_0 E}, \quad (8)$$

where  $I$  is the radiance reflected by the Earth atmosphere (in  $\text{W m}^{-2} \text{sr}^{-1} \text{nm}^{-1}$ ),  $E$  is the incident TOA solar irradiance perpendicular to the solar beam (in  $\text{W m}^{-2} \text{nm}^{-1}$ ), and  $\mu_0$  is the cosine of the solar zenith angle  $\theta_0$ . The viewing zenith angle is denoted as  $\theta$ , the relative azimuth angle as  $\phi - \phi_0$ , and the single scattering angle as  $\Theta$ .

### 3 Description of GOME-2

#### 3.1 Instrument

The spectrometer GOME-2 (Callies et al., 2000) was launched on 19 October 2006 onboard the MetOp-A satellite. The MetOp-A satellite is kept in a polar sun-synchronous orbit at an altitude of 800 km, with a local crossing time of the equator of 9.30 a.m. for the descending node. MetOp-A was launched as the first satellite in a series of three Meteorological Operational (MetOp) satellites. The second satellite platform, MetOp-B, was launched successfully in September 2012, and placed in the same orbit as MetOp-A but with a head start of 50 min (half an orbit) on MetOp-A. The third MetOp satellite, MetOp-C, is scheduled to be launched in 2017. All three MetOp satellites host identical versions of the GOME-2 instrument.

GOME-2, like its predecessor GOME (in this paper also called GOME-1 for clarity) on the ERS-2 satellite (Burrows et al., 1999), measures the sunlight reflected by Earth in the wavelength range between about 240 and 790 nm, with a spectral resolution (FWHM) ranging from 0.2 nm in the UV to 0.4 nm in the NIR. The instrument scans the Earth from east to west in 4.5 s and back in 1.5 s by rotating an internal scanner mirror. The orbit swath sensed this way is 1920 km wide. The typical measurement footprint in the forward scan

is  $80 \text{ km} \times 40 \text{ km}$  (across track  $\times$  along track). The sunlit part of an orbit track consists of about 11 000 measurement footprints. Global coverage is achieved in three consecutive days.

The scientific goal of the GOME-2 instrument is to perform global measurements of trace gases in troposphere and stratosphere for support of meteorological operations and climate studies. The list of trace gases currently retrieved includes ozone,  $\text{NO}_2$ , BrO,  $\text{SO}_2$  and HCHO. Next to these gases, GOME-2 also monitors aerosol presence and retrieves cloud information.

#### 3.2 GOME-2 polarisation measurements

The GOME-2 instrument is, like its predecessors GOME-1 and SCIAMACHY (Bovensmann et al., 1999), not only sensitive to the intensity of the detected light, but also to its state of polarisation. Other instruments such as OMI (Ozone Monitoring Instrument, Levelt et al., 2006) are equipped with a polarisation scrambler to remove the instrumental polarisation dependence. For the GOME-2 instrument the polarisation sensitivity is corrected for in the on-ground processing. For this purpose, the response of the spectral channels to both the intensity and the polarisation of radiation was measured during on-ground calibration campaigns. This in principle allows a correction, provided, of course, that the polarisation of the incoming light is known.

Knowledge of the state of polarisation of the incident radiation is therefore essential. For this reason, the GOME-2 instruments were equipped with two additional detector arrays to measure the parallel component  $I_{\parallel}$  and the perpendicular component  $I_{\perp}$  of the incident light. From Eqs. (1) and (2) it follows that Stokes fraction  $Q/I$  can be determined from these. Stokes fraction  $U/I$  is not known, but GOME-2 was designed in such a way that the dependence on  $U/I$  is much smaller than the dependence on  $Q/I$ . Moreover,  $U/I$  is not neglected but scaled to  $Q/I$  using the theoretical single scattering ratio  $(U/Q)_{ss}$  (Munro and Lang, 2011).

The two detector arrays on board GOME-2 are officially called polarisation measurement devices (PMDs). PMD-p measures the parallel component  $I_{\parallel}$  and PMD-s measures the perpendicular component  $I_{\perp}$ . Both PMD-p and PMD-s consist of 1024 detector pixels, of which 256 can be read out to produce radiance spectra theoretically spanning the wavelength range 300–1200 nm. In practice, the useful wavelength range is limited to 300–850 nm. The integration time (IT) of the PMDs in this mode is 23.4 ms and the associated footprint size in the forward scan amounts to  $10 \text{ km} \times 40 \text{ km}$  (across track  $\times$  along track). This is eight times smaller than the typical footprint size of the main science channels.

In the normal mode of operation, the detected polarisation spectra are *not* transferred down to Earth. Instead, the spectra are down-linked in 15 programmable spectral bands (Munro and Lang, 2011). This reduces the data rate consumption. The current definition of these 15 PMD bands (Lang, 2010) is given graphically in Fig. 1. Here the top bar shows the

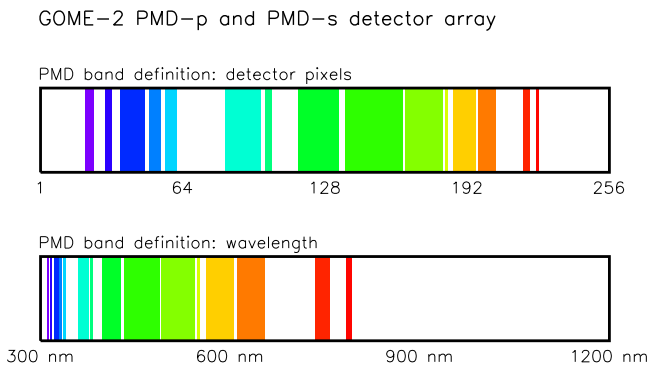


**Figure 1.** Illustration showing the spectral coverage of the fifteen GOME-2 PMD bands, on the PMD detector arrays (top bar), and on the wavelength grid (bottom bar). The PMD RAW mode in principle covers the entire GOME-2 wavelength range between 300 and 800 nm with a spectral resolution ranging between 3 nm in the UV up to 35 nm in the NIR.

definition of the PMD bands in terms of the PMD detector pixels that make up a PMD band. The bottom bar presents the same but then in wavelength space. Note the many PMD bands located in the UV wavelength range. This is a huge improvement over the GOME-1 situation, where only three broadband PMD bands were available for the entire UV–NIR wavelength range.

However, this paper is not concerned with the GOME-2 polarisation measurements that are performed in the normal mode of operation. Our interest is in the so-called “PMD RAW” mode in which the full polarisation spectrum is measured. Employing this mode could only be achieved within roughly the same data rate by reducing the spatial coverage: only every 16th spectrum is actually down-linked, and the 15 spectra before that are discarded. As a result, the footprint size is the same as it is for the normal operation mode. Only one orbit per month is observed in PMD RAW mode.

The PMD RAW spectra that are contained in the GOME-2 level-1b data product are those recorded directly by PMD-p and PMD-s, and are only partly calibrated. The radiances and Stokes fractions  $Q/I$  are not given directly, and they have to be calculated from the PMD-p and PMD-s signals. For this, we follow the description given in the Product Generation Specification (PGS) document (Munro and Lang, 2011) but then adapted to the PMD RAW situation. The steps that are needed to calculate the radiances and Stokes fractions are:

1. Determine the raw signals for PMD-p and PMD-s.
2. Perform a dark current correction.
3. Correct for pixel-to-pixel gain (PPG).
4. Determine the spectral calibration of the PMDs.
5. Perform an etalon correction.
6. Correct for stray light.

7. Determine the viewing and solar angles.
8. Calculate the single scattering  $(U/Q)_{ss}$  ratio.
9. Determine the Mueller matrix elements (MMEs).
10. Calculate Stokes parameter  $Q/I$  using Eq. (167) (PGS-7.0).
11. Calculate the radiance  $I$  using Eq. (216) (PGS-7.0).

Steps 1–7 are already performed for the PMD RAW data inside the GOME-2 level-1b product. The MME key data can be found in the GOME-2 level-1a product. The version of the level-1 data which we used was version 5.3. In this paper, we only present data from 2007 and 2008. Data from later years may be affected by instrument degradation.

#### 4 Case studies and radiative transfer simulations

In this section we study the polarisation measurements that are performed by the GOME-2 instrument in its special PMD RAW mode. We also study the Earth reflectance that may be derived from the PMD measurements in this special observation mode. We do this for a number of cases, and we compare the results with simulations performed by a radiative transfer model. As mentioned before, the PMD RAW mode is only active for one orbit per month, and the orbit paths of all PMD RAW mode orbits collected so far have been nearly identical. In each of the three panels in Fig. 2 the associated orbit swath is drawn over the region containing Northern America. The locations of three scenes that will be studied are indicated by the three white circles.

The three panels in Fig. 2 each have a background that represents the Lambert-equivalent reflectivity (LER) of the surface at 772 nm for the month May, determined from the GOME-1, MERIS, and GOME-2 instruments, respectively (Koelemeijer et al., 2003; Popp et al., 2011). The surface LER is an essential input parameter for the radiative transfer calculations of clear-sky scenes that will be presented in this section and represents the largest source of uncertainty (see, e.g. Tilstra et al., 2005, Fig. 4). Clearly, Fig. 2 poses a warning that there are large differences between the three surface LER databases.

##### 4.1 Case 1

The first case to be studied is that of scene 1 as defined in Fig. 2. The scene was observed on 8 August 2007 around 19:12 UTC and was cloud free at that time. This was checked using AVHRR cloud fraction data, which had been mapped to the GOME-2 footprints. The scene was observed by the last forward-scan PMD RAW measurement inside the respective scan from east to west. In the left panel of Fig. 3 the red curve shows the Earth reflectance spectrum retrieved from the PMD RAW measurements, presented as a function

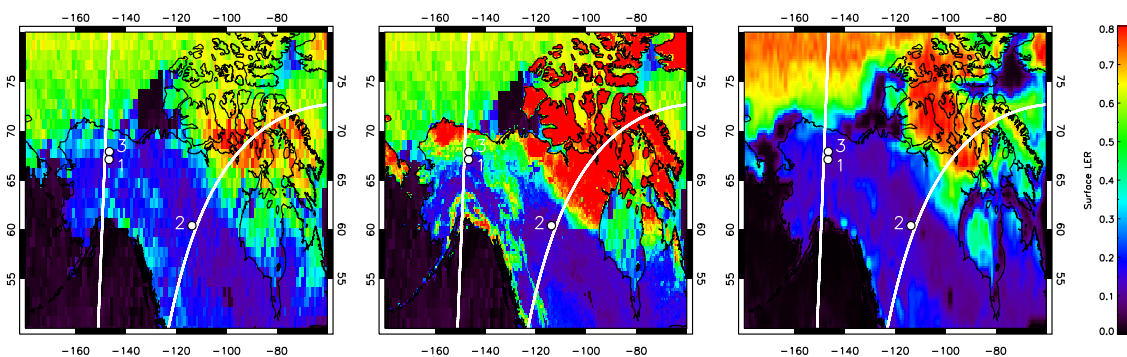


**Figure 2.** Geophysical location of the three cases in North America studied in this paper. Case 1: 67.2° N, 146.3° W; case 2: 60.4° N, 113.6° W; case 3: 67.9° N, 146.3° W. All three cases constitute cloud-free scenes over land. The two white curves indicate the edges of the GOME-2 orbit swath. Each of the three panels contains a different background. This background represents the 772 nm surface LER product of GOME-1, MERIS and GOME-2, respectively, for the month May. Obviously, there are significant differences which can have a large impact on the outcome of the simulations performed in this paper.

of wavelength. The green spectrum was calculated by the radiative transfer code DAK (“Doubling-Adding KNMI”) (de Haan, 1987; Stammes, 2001). All relevant scene parameters that were known were fed to the code. These parameters include ozone column (293 DU, obtained from the TEMIS website, <http://www.temis.nl>), the viewing and solar angles, surface pressure, surface albedo and aerosol optical thickness (AOT).

The surface albedo was taken from the GOME-1 surface LER database (Koelemeijer et al., 2003). Aerosol presence was introduced by including Lowtran-7 tropospheric aerosol. We assumed an AOT value of 0.03, somewhat smaller than the estimated value of 0.05 which we deduced from AOT observations made by the nearby AERONET station of “Bonanza Creek”. Note that the surface albedo of the GOME-1 surface LER database may actually partly represent background aerosol as aerosol presence was not filtered out in the surface LER retrieval (Koelemeijer et al., 2003). Furthermore, to get an as good as possible comparison, we included not only ozone absorption, but also absorption by oxygen ( $O_2$ - $O_2$ ,  $O_2$ -A, and  $O_2$ -B band) and water vapour. From the left panel of Fig. 3 we conclude that there is a reasonable agreement between the measured spectrum and the simulated spectrum, especially in the UV, below 450 nm. Above this wavelength there is certainly some disagreement.

To try to understand the differences between measurement and simulation, we improve the simulated spectrum by taking the slit function of the GOME-2 instrument into account. The response functions of the PMD detector pixels are known and the simulated DAK spectrum was convolved with these (wavelength dependent) slit functions. The result is the dashed blue curve shown in Fig. 3. As can be seen, the features around the  $O_2$ -A and water vapour absorption bands are described accurately by the simulated spectrum. However, the result still points to a quantitative disagreement between measurement and model. This could be a calibration

problem, but it is at this point more likely to be caused by inaccuracies in the provided surface albedo spectrum.

To verify whether inaccuracies in the surface albedo spectrum could indeed explain the differences between measurement and simulation, we redo our analyses using surface albedo input from the GOME-2 and MERIS surface albedo databases. The results are shown in Fig. 3. Here, the solid and dotted blue curves represent simulation results convolved with the PMD slit function and based on the GOME-2 and MERIS surface albedo databases, respectively. Only above 500 nm are there significant differences. The analysis confirms that inaccuracies in the surface albedo have a large impact for the longer wavelengths, and that it is hard to draw quantitative conclusions for wavelengths above 500 nm. Below 500 nm the PMD RAW reflectance is found to be accurate within 2 %.

We now shift our attention to the PMD RAW polarisation measurements. The right panel of Fig. 3 presents the spectrum of the measured Stokes fraction  $Q/I$  (in red). The polarisation spectrum shows a lot of detail. The green horizontal lines indicate the situation of unpolarised light, for which  $Q/I = 0$ , and the situation of singly scattered light, for which  $Q/I = (Q/I)_{ss}$ . For most of the wavelengths, the measured Stokes fraction is found to lie in between these two limits, as one would expect based on considerations given in Krijger et al. (2005). For part of the wavelength range, however, this rule of thumb is violated, because of multiple scattering of the light. To further study the spectrum, we plot the simulated Stokes fraction spectrum (in green) and also the three convolved versions (in blue). The conclusion is that there is a good agreement between the measured and the simulated polarisation spectra for all wavelengths. The spectrum nicely demonstrates the depolarising effect of the surface (albedo) on the Stokes fraction. A feature is present in the polarisation spectrum around 800 nm. Note that the simulated spectrum also violates the rule of thumb mentioned earlier.

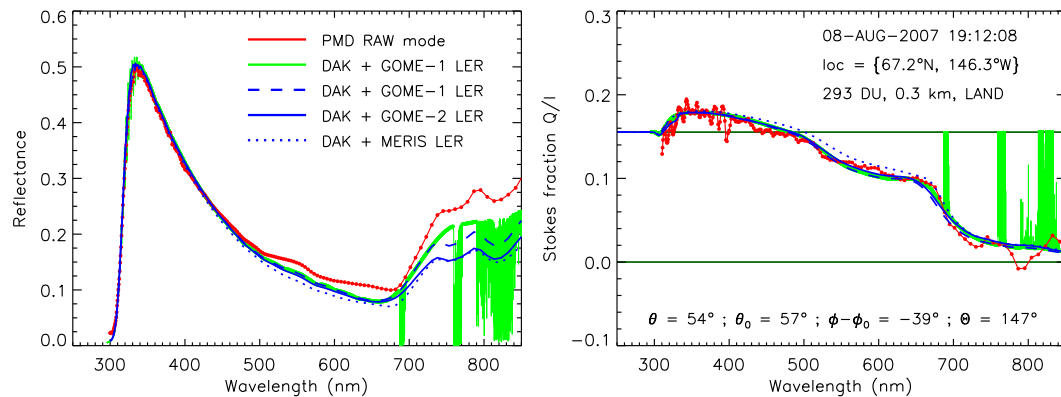


**Figure 3.** Earth reflectance (left panel) and polarisation Stokes fraction  $Q/I$  (right panel) derived from GOME-2 PMD RAW mode measurements for case 1 in Fig. 2 (in red). The green curves represent the high-resolution simulated reflectance and polarisation spectra, based on surface albedo input from the GOME-1 surface LER database. The dashed blue curve represent the same, but convolved with the PMD slit function. The FWHM of this slit function typically ranges between 3 nm in the UV up to 35 nm in the NIR. The solid and dotted blue curves also represent convolved simulation results but for these simulations the surface albedo input was taken from the GOME-2 and MERIS surface reflectivity databases, respectively. The two horizontal green lines in the right panel indicate the unpolarised situation, for which  $Q/I = 0$ , and the single scattering situation, for which  $Q/I = (Q/I)_{ss}$ .

#### 4.2 Case 2

The reflectance spectrum that was measured for scene 2 is shown in the left panel of Fig. 4, again in red. This time the scene was observed by the first forward-scan PMD RAW measurement inside the scan from east to west, leading to an entirely different scattering geometry than for scene 1. The difference with respect to the spectrum of Fig. 3 is mostly caused by a difference in surface albedo, though. The simulation results that are represented in Fig. 4 by the blue curves were all convolved with the PMD slit function, but different surface albedo spectra were used in the radiative transfer calculations. The dashed curve represents the case calculated with the GOME-1 surface LER, the solid curve was calculated using the GOME-2 surface LER, and the dotted one using the surface albedo from the MERIS database. Clear from Fig. 4 is that the particular choice of surface albedo input for the radiative transfer model (RTM) is essential at the longer wavelengths (say, above 400 nm). Apparently, there are quite some differences in the surface albedo databases (such differences were visualised already in Fig. 2). From the comparison between the GOME-2 measured and simulated reflectances we have to conclude that there seems to be a satisfactory agreement when we take into account the uncertainty in surface albedo.

We now look at the spectrum of the Stokes fraction  $Q/I$  which is given in the right panel of Fig. 4. Because of the difference in scattering geometry, the shape of the polarisation spectrum is very different from the one shown in Fig. 3. The simulated polarisation spectra, convolved with the PMD slit function and given in blue, are in reasonable agreement for all three surface albedo inputs. There is quite a good agreement with the measured  $Q/I$ , with

a maximum disagreement of 0.05. This maximum disagreement is found for the longer wavelengths (above 650 nm), and is perhaps caused by the fact that we have a Lambertian (non-polarising) surface included in the simulations. This underestimates the contribution of the surface to the TOA polarisation. However, the non-Lambertian (polarising) nature of the real surface cannot explain the feature that is found around 800 nm. The existence of this feature is pointing to a discrepancy in the GOME-2 calibration key data.

#### 4.3 Case 3

The results for scene 3 are shown in Fig. 5. The scene was observed by the westernmost PMD RAW measurement inside the scan. For the reflectance we find good agreement with the simulations based on the GOME-1, GOME-2, and MERIS surface albedos. Deviations are very small in the UV, but go up to 0.05 in the visible wavelength range. These deviations are explained completely by the uncertainty in the surface LER spectra used. For the scattering geometry at hand, the degree of polarisation is modest. The simulated and measured  $Q/I$  are close together for each of the three surface albedo input spectra. The GOME-2 surface LER seems to generate the best results. There clearly is a wavelength-dependent difference between measurement and simulation. This small difference (of up to 0.02 in  $Q/I$ ) may be explained by inaccuracies in the (assumed) surface albedo, or it may be partly a consequence of the Lambertian (unpolarised) surface reflection. Note that the feature around 800 nm is again present in the polarisation spectrum.

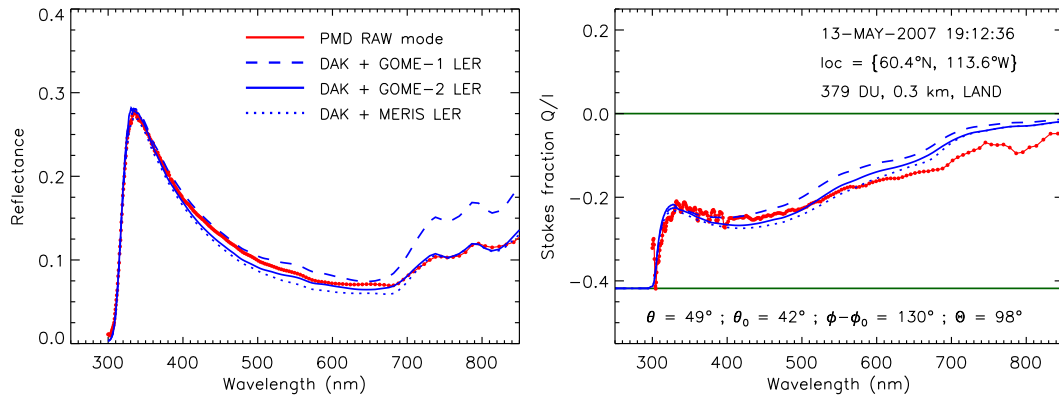


**Figure 4.** Earth reflectance and polarisation Stokes fraction  $Q/I$  measured by GOME-2 for case 2 indicated in Fig. 2 (in red). The simulated spectra (in blue) were calculated with different surface albedo inputs (see legend) and were convolved with the PMD slit function. For the Stokes fraction  $Q/I$  the agreement between measurement and simulation is good in the UV but less good for the longer wavelengths.

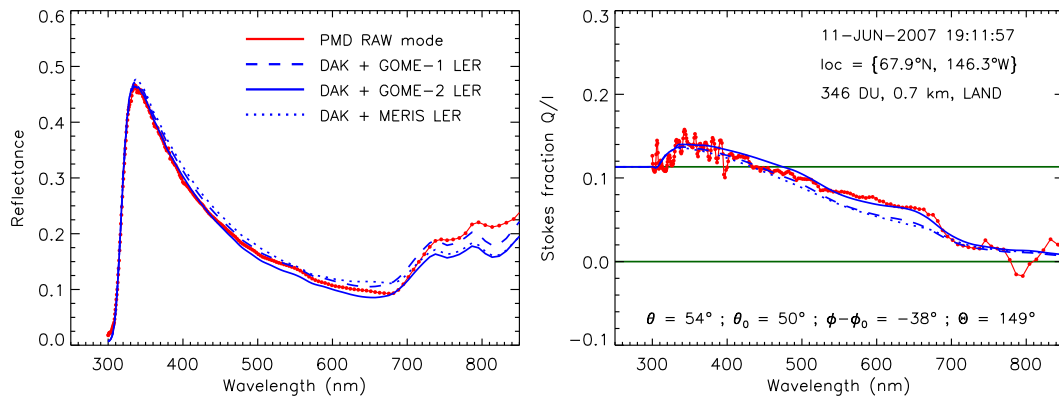


**Figure 5.** Reflectance and polarisation spectrum measured by GOME-2 for case 3. The agreement between measurement and simulation is good for both reflectance and polarisation for all three surface albedo inputs.

## 5 Special polarisation geometries

In the previous section the goal was to verify the GOME-2 PMD RAW polarisation measurements by comparison with simulations. The quality of the simulated reflectance and polarisation is limited by the uncertainty in the surface albedo. This is especially the case for the longer (visible) wavelengths, where the impact of the surface albedo is the largest. Because of this, the focus was restricted to cloud-free scenes over land. In this section, we do not use radiative transfer calculations, but employ a method which focuses on special scattering geometries for which the Stokes fraction  $Q/I$  can be expected to be close to zero based on geometrical considerations (see, for instance, Aben et al., 2003).

This special geometry method relies on the knowledge that the direction of linear polarisation  $\chi$  in most situations deviates very little from its theoretical single scattering value  $\chi_{ss}$  (Schutgens et al., 2004). This means that we can use  $\chi \approx \chi_{ss}$ , where  $\chi_{ss}$  is calculated from geometry only (Tilstra et al., 2003). Picking out all scenes for which  $\chi_{ss}$  is close to  $45^\circ$  or

$135^\circ$  we end up with a collection of “validation” scenes for which  $Q/I$  should be close to zero irrespective of the value of the degree of linear polarisation  $P$  (see Eq. 4). Strictly speaking, this only validates the subset of measurements and scattering geometries for which  $Q/I \approx 0$ . However, a study (Tilstra, 2008) has shown that, at least for the GOME-2 PMD bands, the quality of the  $Q/I$  for these special geometries is comparable to the quality of  $Q/I$  for all scattering geometries.

In Fig. 6 we present the Earth reflectance of one of the GOME-2 PMD RAW special geometry observations. In this case the scene was selected also based on the grounds that it was located over sea and cloud free at the time of measurement. The results of radiative transfer calculations are also given, in the same way as was done for Fig. 3. There seems to be a reasonable agreement. However, at 750 nm measurement and simulation of the reflectance differ from each other by more than 0.01 ( $\sim 25\%$ ). In Fig. 6 we also show the Stokes fraction  $Q/I$  of the same scene. The simulation results are not shown, because accurate modelling

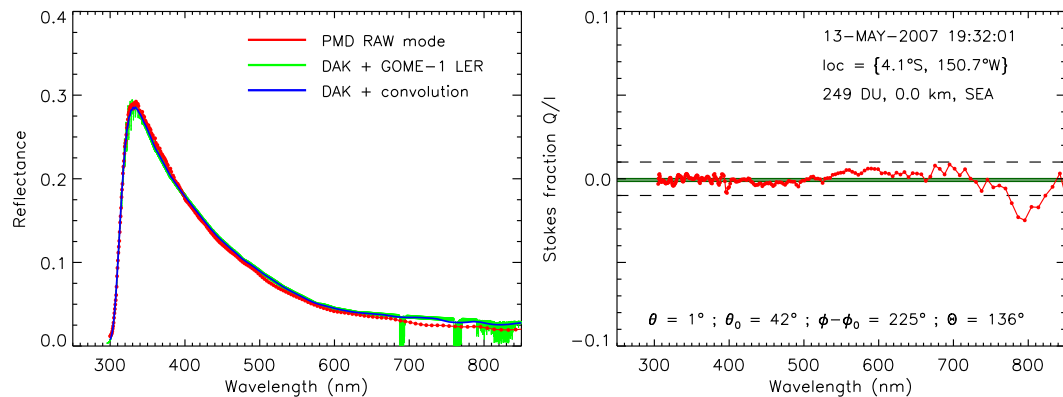


**Figure 6.** Left: reflectance spectrum measured by GOME-2 for a special geometry case over the ocean for which we expect  $Q/I$  to be close to zero based on geometrical considerations. The agreement between measurement and simulation is good. Right: polarisation Stokes fraction  $Q/I$ . Here the simulation results are not shown. Instead, the brown horizontal lines indicate the small range in Stokes fractions in which we expect to find the  $Q/I$  measurement. The dashed horizontal lines indicate the 0.01 accuracy level.

in the visible under these conditions (low surface albedo) is not possible anyway. Instead, two horizontal brown lines that indicate the  $Q = 0$  and  $Q = (Q/I)_{ss}$  limits are shown and, as explained, the red PMD RAW special geometry measurements are expected to fall in between these two limits:  $Q/I \approx 0$ . This is almost completely the case. Some deviation is certainly there, though, and the spectral shape of the discrepancy resembles the spectral shape of the differences between measurement and simulation presented in the previous section, where the measured Stokes fraction  $Q/I$  was compared with simulated  $Q/I$ . From this we conclude that the Stokes fraction  $Q/I$  – of the PMD RAW mode – is suffering from detectable radiometric calibration problems. The problems are not large: the accuracy of  $Q/I$  appears to be within 0.01 for most wavelengths, which is well within the pre-flight expected accuracy of  $\pm 0.05$ . The dashed horizontal lines in Fig. 6 indicate the “0.01” accuracy levels.

In the left panel of Fig. 7 we present the measured Stokes fraction spectrum for all collected special geometry observations in the years 2007 and 2008. The selection criteria used were  $|\cos 2\chi_{ss}| < 0.005$  and  $\Theta < 175^\circ$ , which resulted in a total of 470 spectra. The second criterion on the single scattering angle  $\Theta$  was added to filter out backscatter geometries. Also given, in black, is the mean of the spectra, and the standard deviation  $\sigma$ , visualised by the two blue curves. The result confirms that there are indeed spectral features present in the Stokes fractions. Further analyses of the data did not point to a clear dependence on, for instance, viewing angle.

An alternative validation approach is to focus on backscatter geometries. For these situations, where  $\Theta \simeq 180^\circ$ , the degree of linear polarisation  $P$  may be expected to be small based on symmetry arguments, resulting in  $Q/I$  close to zero independent of the properties of the scene. The right panel of Fig. 7 presents the measured Stokes fraction spectra for all collected backscatter geometry observations in the years 2007 and 2008. This time we used the selection criterion

$\Theta > 178^\circ$  and  $|\cos 2\chi_{ss}| > 0.03$ , where the second criterion makes sure that there is no overlap with the special geometry observations presented in the left panel of Fig. 7. A total of 155 backscatter geometry spectra were found. Comparing the results with the results in the left panel of Fig. 7 we see that there are clear differences. Especially in the UV, below  $\sim 400$  nm, the backscatter observations systematically show an offset in  $Q/I$ .

This discrepancy is, however, not caused by imperfections in the GOME-2 data. It is a result of the fact that backscatter geometries do not always lead to completely unpolarised light. To explain, for backscatter situations where  $\theta = \theta_0 > 0$  the axis of rotational symmetry (with respect to the scattering geometry) makes an angle with the zenith axis, which is the symmetry axis of rotational symmetry of the atmosphere. In this situation the multiple scattering terms do not cancel out any more, and the backscattered light at the TOA is not completely unpolarised. This phenomenon is captured well by radiative transfer simulations. The result of such a (representative) calculation is given by the brown spectrum in the right panel of Fig. 7. Therefore, backscatter geometries in general do not always lead to completely unpolarised light and the  $Q/I$  to be expected is in general small but not zero. Note that a similar effect is present for the special geometry situations shown in the left panel of Fig. 7. A calculation of  $Q/I$  for a representative special geometry situation is given here by the brown spectrum. Taking all this into account explains most of the discrepancies between the two results in Fig. 7. The conclusion is that both approaches point to the same systematic spectral features and indicate that the error on Stokes fraction  $Q/I$  is below 0.01 for most wavelengths.

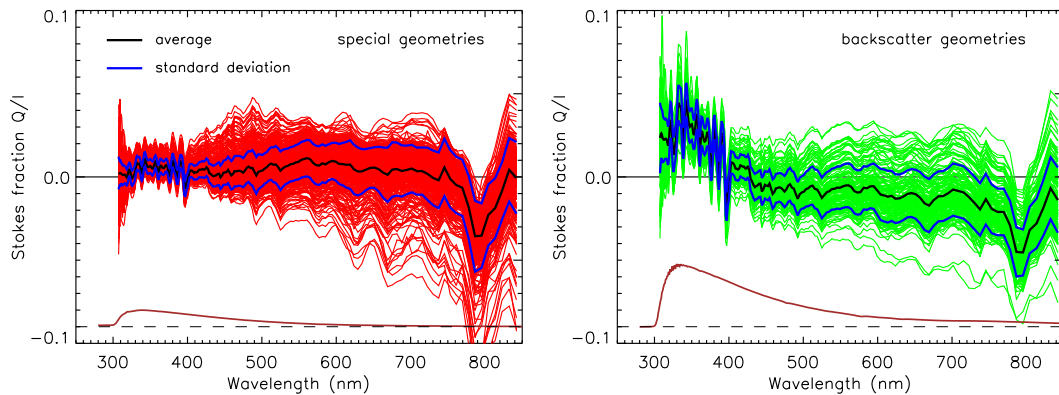


**Figure 7.** Left: Stokes fraction  $Q/I$  for special geometries along the GOME-2 PMD RAW orbit for which we expect  $Q/I$  to be close to zero based on geometrical considerations. The plot shows 470 spectra, their mean, and the standard deviation  $\sigma$ . Right: Stokes fraction  $Q/I$  for 155 backscatter geometries for which we expect  $Q/I$  to be close to zero based on symmetry arguments. Brown curves (shifted downwards by 0.09 for clarity): simulated  $Q/I$  for a typical special geometry/backscatter geometry, showing that the expected  $Q/I$  is not completely equal to zero.

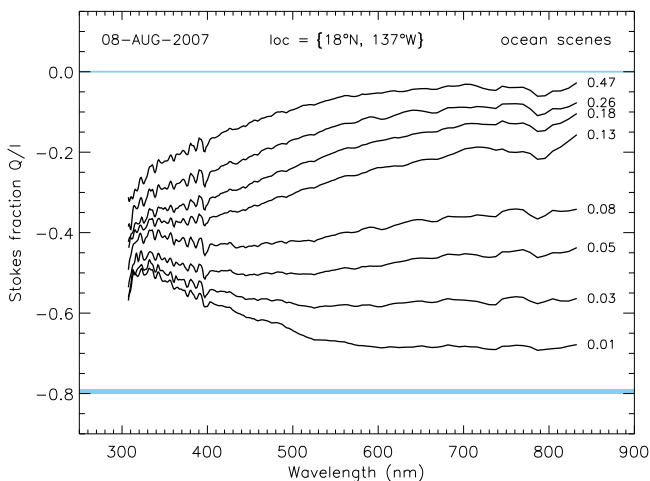


**Figure 8.** Stokes fraction  $Q/I$  as a function of wavelength for ocean scenes with various degrees of cloud contamination but otherwise comparable conditions. The numbers indicate effective cloud fractions. The blue horizontal lines are explained in the text.

## 6 Earth polarisation spectra

In this section we illustrate the potential of using the GOME-2 PMD RAW mode for the study of high-resolution Earth polarisation spectra. For this, we study the Stokes fraction  $Q/I$  spectrum of a few typical Earth scenes under typical conditions. In Fig. 8 we present eight scenes observed over the ocean with different degrees of cloud cover, but with otherwise comparable conditions. The eight observations were recorded within a time interval of three minutes (27 scans) and for the exact same scan mirror angle. Therefore, the viewing and solar geometries are very similar and so are the single scattering angles and the theoretical single

scattering Stokes fractions. The range in  $(Q/I)_{ss}$  is illustrated graphically in Fig. 8 by the horizontal blue bar.

For the spectra an effective cloud fraction  $c_{\text{eff}}$  is provided to give an idea of the cloudiness of the scenes. This effective cloud fraction was calculated for the PMD RAW footprints in a way similar to that followed in the FRESCO retrieval algorithm (Wang et al., 2008), with the difference that the retrieval was fed beforehand with the official FRESCO cloud pressure that was measured for the (eight times) bigger main science channel footprints. This approach was needed as the  $\text{O}_2\text{-A}$  band is not resolved properly by the PMD RAW mode measurements, allowing only cloud fraction to be derived for the smaller PMD RAW footprints.

The nearly cloud-free spectrum ( $c_{\text{eff}} = 0.01$ ) shows the typical wavelength behaviour of atmospheric polarisation over a relatively dark surface: just above 300 nm depolarisation sets in rapidly caused by the onset of multiple Rayleigh scattering and the increased surface reflection, both made visible by the decrease of ozone absorption. As the wavelength increases further, the Rayleigh optical thickness decreases further and, because of the low surface albedo, single Rayleigh scattering is again the dominant process. As a result, the spectrum moves in the direction of the single scattering limit  $(Q/I)_{ss}$  again.

With increasing cloud cover (i.e. with increasing  $c_{\text{eff}}$ ), the depolarisation increases, and the curves are positioned closer to the line  $Q/I = 0$  (given in blue). For the longer wavelengths, this effect is larger than for the shorter wavelengths because of the lower atmospheric contribution. At the highest effective cloud fraction ( $c_{\text{eff}} = 0.47$ ) the scene is dominated entirely by the high reflectivity of the (mainly depolarising) cloud layer. The picture shown in Fig. 8 by the eight traces is quite generic in the sense that the traces describe the typical behaviour of  $Q/I$  for scenes over the ocean with variable cloudiness.

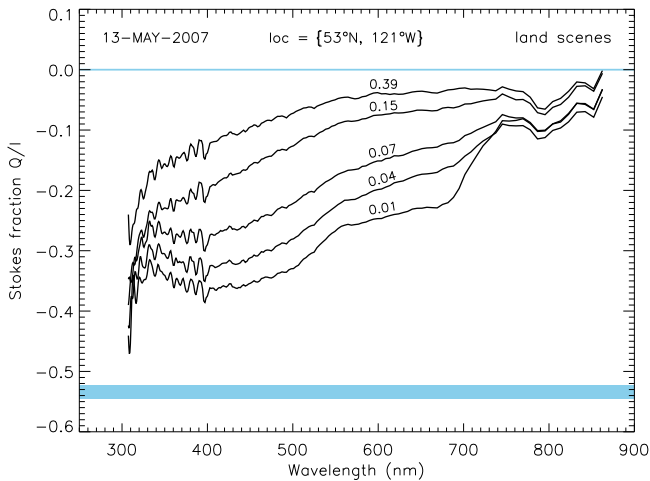


**Figure 9.** Spectra of  $Q/I$  for scenes over (vegetated) land. Cloud presence varies from one scene to the other. For the rest the scene properties are comparable. As before, the numbers indicate effective cloud fractions. For low effective cloud fractions the spectra show the chlorophyll “bump” at  $\sim 500$  nm and the vegetation red edge at  $\sim 700$  nm.

Now we focus on a selection of scenes over land with various degrees of cloud coverage. The resulting  $Q/I$  spectra are given in Fig. 9. Again the scenes were taken at the same position of the scanner mirror. The time interval in which the measurements were performed was smaller than in the ocean case (8 scans; less than one minute). The range in the calculated  $(Q/I)_{ss}$ , illustrated by the blue bar, is a bit larger, due to the higher solar zenith angles. Nevertheless, the scenes are highly comparable, apart from the (selected) differences in cloud cover. An effective cloud fraction  $c_{eff}$  as indication of this cloud cover is provided in Fig. 9 for each scene.

In the nearly cloud-free spectrum ( $c_{eff} = 0.01$ ) we can discern the typical wavelength behaviour of atmospheric polarisation over a (mainly depolarising) surface of type “vegetation” (see, for instance, Aben et al., 2003). As in the ocean case, the  $Q/I$  spectrum moves away from the single scattering value  $(Q/I)_{ss}$  as the wavelength exceeds 300 nm, and around 330 nm it slowly starts to bend back. The major difference compared to the ocean case is that the surface albedo of vegetated land is higher than that of the ocean for wavelengths above about 400 nm. As the surface is mostly depolarising,  $Q/I$  starts to move towards the unpolarised limit  $Q/I = 0$  again, at a rate controlled mainly by the magnitude of the surface albedo. In Fig. 9 we clearly see the  $Q/I$  spectrum for  $c_{eff} = 0.01$  respond to the chlorophyll “bump” at  $\sim 500$  nm and the vegetation red edge at  $\sim 700$  nm.

Looking at the traces with higher  $c_{eff}$ , we see that the features introduced by the shape of the “vegetation” albedo spectrum fade away from the  $Q/I$  spectra. The spectra basically start to adopt the shape of the  $Q/I$  spectra of the clouded ocean scenes. Note that the (probably instrumental)

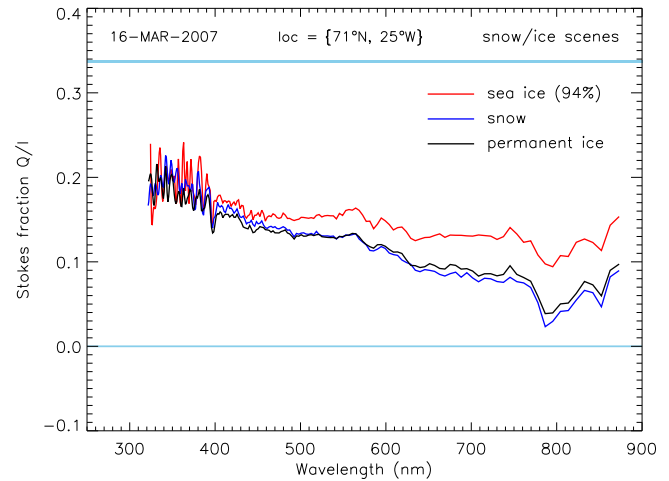


**Figure 10.** Stokes fraction  $Q/I$  for cloud-free scenes over snow (blue), permanent ice (black) and sea ice (red).

feature around 800 nm that was discussed in Sect. 4 is clearly present in all the spectra presented in Fig. 9.

Finally, in Fig. 10 we study the TOA  $Q/I$  spectrum of snow and ice surfaces. More precisely, the surfaces studied are “snow”, “permanent ice” and “sea ice”. All three scenes were cloud free, and taken at the same scan mirror position and within 34 scans ( $\sim 3$  min). Clearly, the spectra of snow and permanent ice mimic each other in great detail. The sea ice case shows a higher  $Q/I$  for wavelengths above 400 nm. This can be explained by the lower albedo of sea ice compared to the albedo of snow or pure ice. This leads to a higher degree of polarisation as explained earlier. On the other hand, the surface can also actively contribute to the polarisation of the scene. Spectra as in Fig. 10 can provide information on the polarisation contribution of the snow/ice surface.

In conclusion, the GOME-2 PMD RAW mode can provide high-quality high-resolution Earth polarisation spectra.

## 7 Parameterisation of UV polarisation

The GOME-2 PMD RAW mode provides unique measurements of the polarisation spectrum at the top of the atmosphere. According to Schutgens and Stammes (2002) the degree of polarisation  $P$  in the UV wavelength range can be parameterised using a generalised distribution function (GDF). Essentially, the TOA degree of polarisation  $P$  can be well described (in the UV) by the following function:

$$P(\lambda) = \begin{cases} P_{ss}, & \lambda \leq \lambda_{ss}, \\ P_{ss} - \alpha \left( 1 - \frac{4e^{-(\lambda-\lambda_{ss})/\Delta\lambda}}{(1+e^{-(\lambda-\lambda_{ss})/\Delta\lambda})^2} \right), & \lambda > \lambda_{ss}, \end{cases} \quad (9)$$

where  $\lambda$  is the wavelength, and  $\alpha$ ,  $\lambda_{ss}$  and  $\Delta\lambda$  are in principle fit parameters. Parameterisations for  $\lambda_{ss}$  and  $\Delta\lambda$  are, however, provided in the referenced paper. As explained in this

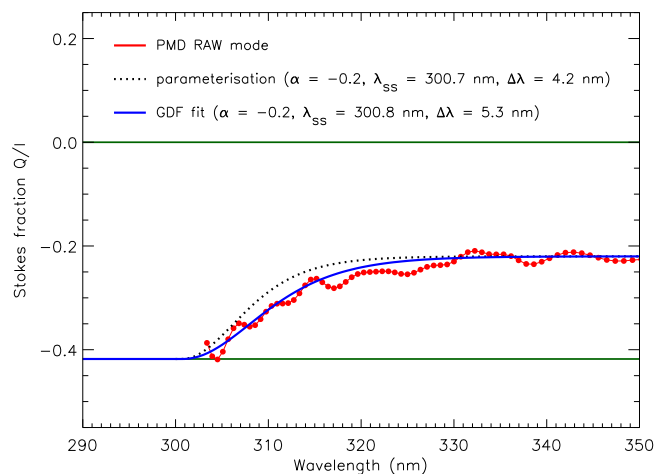


**Figure 11.** Polarisation Stokes fraction  $Q/I$  for scene 2 defined in Fig. 2 (red points) and GDF function based on parameterisation (blue curve). Fit parameters are given in the plot. The agreement is good.

reference, expressions similar to Eq. (9) can be written down for the Stokes fractions  $Q/I$  and  $U/I$ .

The idea by Schutgens and Stammes (2002) to propose the GDF as a description of the UV polarisation originated from a study of simulated polarisation spectra. In Fig. 11 we verify the correctness of Eq. (9) using GOME-2 PMD RAW polarisation data. The figure presents the measured Stokes fraction  $Q/I$  already shown in Fig. 4, but now accompanied by a blue curve which represents the GDF defined in Eq. (9). The fit parameters were  $\alpha = -0.20$ ,  $\lambda_{ss} = 300.8$  nm, and  $\Delta\lambda = 5.3$  nm. Schutgens and Stammes (2002) provide a recipe for calculating the parameters  $\lambda_{ss}$  and  $\Delta\lambda$ . Following this recipe, using a geometrical air-mass factor  $M$  of 2.9 and a surface albedo  $A$  of 0.05, we find  $\lambda_{ss} = 300.7$  nm and  $\Delta\lambda = 4.2$  nm. The fit based on these numbers is represented in Fig. 11 by the dotted curve. The differences may be explained by the fact that the scene is observed from an off-nadir viewing geometry ( $\mu = 0.65$ ), while the referenced paper is restricted to scenes for which  $\mu > 0.92$ .

Nevertheless, the agreement between the GDF and the measured polarisation spectrum is good, except for the spectral features that are seen in the measured polarisation spectrum. These features are not caused by ozone absorption, but presumably by (i) spectral misalignment between the two PMD detector arrays and (ii) inaccuracies in the radiometric calibration. Outside the UV these spectral features are seen to disappear. It is important to understand the origin of these spectral features and this should be investigated in the future.

In summary, the above result confirms that the UV polarisation spectrum can indeed be described by the proposed GDF.

## 8 Conclusions

The spectra of Stokes fraction  $Q/I$  measured by GOME-2 in its PMD RAW mode and studied in this paper are the first high-resolution top of atmosphere contiguous polarisation spectra covering the entire UV–NIR wavelength range between 300 and 850 nm. The GOME-2 polarisation spectra may be useful to the validation of polarised radiative transfer models and to the development of satellite instruments. This paper started with a validation of the Stokes fraction spectra using radiative transfer calculations and a method based on special geometries. From the validation results we concluded that the polarisation spectra are of good quality:  $Q/I$  is accurate within 0.01 for most wavelengths. There is also room for improvement – we mention explicitly the feature around 800 nm which points to a systematic error in the radiometric calibration and the spectral features that are seen in the UV. The origin of the spectral features in the UV needs to be further investigated.

Using the high-resolution spectra of Stokes fraction  $Q/I$  recorded in the GOME-2 PMD RAW mode we studied the behaviour of atmospheric polarisation for typical scenes over sea, (vegetated) land and snow/ice surfaces. The behaviour could be explained qualitatively and the measured traces, observed for various degrees of cloud cover, provide a conceptual model of the Earth's polarisation. As an example of the potential of the PMD RAW mode, we made use of the high spectral resolution in the UV to test if the polarisation can be described in terms of a generalised distribution function (GDF). This is indeed the case.

*Acknowledgements.* The work presented in this publication was financed by EUMETSAT via the O3M SAF. EUMETSAT is also acknowledged for providing the GOME-2 data. We acknowledge the use of AERONET data and thank John R. Vande Castle for his effort in establishing and maintaining the Bonanza Creek site. Michael Eisinger (ESA) is acknowledged for this contribution to the construction and design of the polarisation measurement capabilities of the GOME-2 instrument.

Edited by: C. von Savigny

## References

- Aben, I., Helderma, F., Stam, D. M., and Stammes, P.: Spectral fine-structure in the polarisation of skylight, *Geophys. Res. Lett.*, 26, 591–594, doi:10.1029/1999GL900025, 1999.
- Aben, I., Tanzi, C. P., Hartmann, W., Stam, D. M., and Stammes, P.: Validation of space-based polarization measurements by use of a single-scattering approximation, with application to the Global Ozone Monitoring Experiment, *Appl. Optics*, 18, 3610–3619, doi:10.1364/AO.42.003610, 2003.
- Bates, D. R.: Rayleigh scattering by air, *Planet. Space Sci.*, 32, 785–790, doi:10.1016/0032-0633(84)90102-8, 1984.
- Boesche, E., Stammes, P., Ruhtz, T., Preusker, R., and Fischer, J.: Effect of aerosol microphysical properties on polarization of

- skylight: sensitivity study and measurements, *Appl. Optics*, 45, 8790–8805, doi:10.1364/AO.45.008790, 2006.
- Bovensmann, H., Burrows, J. P., Buchwitz, M., Frerick, J., Noël, S., Rozanov, V. V., Chance, K. V., and Goede, A. P. H.: SCIAMACHY: mission objectives and measurement modes, *J. Atmos. Sci.*, 56, 127–150, 1999.
- Burrows, J. P., Weber, M., Buchwitz, M., Rozanov, V., Ladstätter-Weißenmayer, A., Richter, A., de Beek, R., Hoogen, R., Bramstedt, K., Eichman, K.-U., Eisinger, M., and Perner, D.: The Global Ozone Monitoring Experiment (GOME): mission concept and first scientific results, *J. Atmos. Sci.*, 56, 151–175, 1999.
- Callies, J., Corpaccioli, E., Eisinger, M., Hahne, A., and Lefebvre, A.: GOME-2 – Metop's second-generation sensor for operational ozone-monitoring, *ESA Bull.-Eur. Space*, 102, 28–36, 2000.
- Chandrasekhar, S.: Radiative Transfer, Dover Publications, Mineola, New York, 1960.
- Coulson, K. L.: Polarization and Intensity of Light in the Atmosphere, A. Deepak Publishing, Hampton, Virginia, 1988.
- de Haan, J. F., Bosma, P. B., and Hovenier, J. W.: The adding method for multiple scattering calculations of polarized light, *Astron. Astrophys.*, 183, 371–391, 1987.
- Deschamps, P.-Y., Bréon, F.-M., Leroy, M., Podaire, A., Brickaud, A., Buriez, J.-C., and Sèze, G.: The POLDER mission: instrument characteristics and scientific objectives, *IEEE T. Geosci. Remote*, 32, 598–615, 1994.
- Deuzé, J. L., Bréon, F.-M., Devaux, C., Goloub, P., Herman, M., Lafrance, B., Maignan, F., Marchand, A., Nadal, F., Perry, G., and Tanré, D.: Remote sensing of aerosols over land surfaces from POLDER-ADEOS-1 polarized measurements, *J. Geophys. Res.*, 106, 4913–4926, doi:10.1029/2000JD900364, 2001.
- Hasekamp, O. P. and Landgraf, J.: Retrieval of aerosol properties over land surfaces: capabilities of multiple-viewing-angle intensity and polarization measurements, *Appl. Optics*, 46, 3332–3344, doi:10.1364/AO.46.003332, 2007.
- Hovenier, J. W., van der Mee, C., and Domke, H.: Transfer of Polarized Light in Planetary Atmospheres, Kluwer Academic Publishers, Dordrecht, the Netherlands, 2004.
- Koelemeijer, R. B. A., de Haan, J. F., and Stammes, P.: A database of spectral surface reflectivity in the range 335–772 nm derived from 5.5 years of GOME observations, *J. Geophys. Res.*, 108, 4070, doi:10.1029/2002JD002429, 2003.
- Krijger, J. M., Tanzi, C. P., Aben, I., and Paul, F.: Validation of GOME polarization measurements by method of limiting atmospheres, *J. Geophys. Res.*, 110, D07305, doi:10.1029/2004JD005184, 2005.
- Kuze, A., Suto, H., Nakajima, M., and Hamazaki, T.: Thermal and near infrared sensor for carbon observation Fourier-transform spectrometer on the Greenhouse Gases Observing Satellite for greenhouse gases monitoring, *Appl. Optics*, 48, 6716–6733, doi:10.1364/AO.48.006716, 2009.
- Lang, R.: GOME-2 PMD band definitions 3.0 and PMD calibration, Doc. No. EUM/OPS-EPS/DOC/07/0601, Issue 8, 11 June, EUMETSAT, Darmstadt, Germany, 2010.
- Levelt, P. F., van den Oord, G. H. J., Dobber, M. R., Mälkki, A., Visser, H., de Vries, J., Stammes, P., Lundell, J. O. V., and Saari, H.: The Ozone Monitoring Instrument, *IEEE T. Geosci. Remote*, 44, 1093–1101, doi:10.1109/TGRS.2006.872333, 2006.
- Lichtenberg, G., Kleipool, Q., Krijger, J. M., van Soest, G., van Hees, R., Tilstra, L. G., Acarreta, J. R., Aben, I., Ahlers, B., Bovensmann, H., Chance, K., Gloudemans, A. M. S., Hoogeveen, R. W. M., Jongma, R. T. N., Noël, S., Pitters, A., Schrijver, H., Schrijvers, C., Sioris, C. E., Skupin, J., Slijkhuis, S., Stammes, P., and Wuttke, M.: SCIAMACHY Level 1 data: calibration concept and in-flight calibration, *Atmos. Chem. Phys.*, 6, 5347–5367, doi:10.5194/acp-6-5347-2006, 2006.
- Mishchenko, M. I. and Travis, L. D.: Satellite retrieval of aerosol properties over the ocean using polarization as well as intensity of reflected sunlight, *J. Geophys. Res.*, 102, 16989–17013, doi:10.1029/96JD02425, 1997.
- Munro, R. and Lang, R.: GOME-2 Level 1 Product Generation Specification, Doc. No. EPS.SYS.SPE.990011, Issue 7.0, 28 February, EUMETSAT, Darmstadt, Germany, available at: [http://www.eumetsat.int/website/wcm/idc/idcplg?IdcService=GET\\_FILE&dDocName=pdf\\_ten\\_990011-eps-gome-pgs&RevisionSelectionMethod=LatestReleased&Rendition=Web](http://www.eumetsat.int/website/wcm/idc/idcplg?IdcService=GET_FILE&dDocName=pdf_ten_990011-eps-gome-pgs&RevisionSelectionMethod=LatestReleased&Rendition=Web), 2011.
- Popp, C., Wang, P., Brunner, D., Stammes, P., Zhou, Y., and Grzegorski, M.: MERIS albedo climatology for FRESCO+ O<sub>2</sub> A-band cloud retrieval, *Atmos. Meas. Tech.*, 4, 463–483, doi:10.5194/amt-4-463-2011, 2011.
- Schutgens, N. A. J. and Stammes, P.: Parametrisation of Earth's polarisation spectrum in the ultra-violet, *J. Quant. Spectrosc. Ra.*, 75, 239–255, doi:10.1016/S0022-4073(01)00248-5, 2002.
- Schutgens, N. A. J. and Stammes, P.: A novel approach to the polarization correction of spaceborne spectrometers, *J. Geophys. Res.*, 108, 4229, doi:10.1029/2002JD002736, 2003.
- Schutgens, N. A. J., Tilstra, L. G., Stammes, P., and Bréon, F.-M.: On the relationship between Stokes parameters  $Q$  and  $U$  of atmospheric ultraviolet/visible/near-infrared radiation, *J. Geophys. Res.*, 109, D09205, doi:10.1029/2003JD004081, 2004.
- Stammes, P.: Spectral radiance modelling in the UV-visible range, in: *IRS 2000: Current Problems in Atmospheric Radiation*, edited by: Smith, W. L. and Timofeyev Y. M., A. Deepak Publishing, Hampton, Virginia, 385–388, 2001.
- Tanré, D., Bréon, F. M., Deuzé, J. L., Dubovik, O., Ducos, F., François, P., Goloub, P., Herman, M., Lifermann, A., and Waquet, F.: Remote sensing of aerosols by using polarized, directional and spectral measurements within the A-Train: the PARASOL mission, *Atmos. Meas. Tech.*, 4, 1383–1395, doi:10.5194/amt-4-1383-2011, 2011.
- Tilstra, L. G.: GOME-2 Polarisation Study – Final report, Doc. No. SRON-EOS-RP-08-033, Issue 0.3, 22 December, SRON, Utrecht, the Netherlands, available at: <http://www.knmi.nl/~tilstra/> (last access: 4 July 2014), 2008.
- Tilstra, L. G. and Stammes, P.: Alternative polarisation retrieval for SCIAMACHY in the ultraviolet, *Atmos. Chem. Phys.*, 5, 2099–2107, doi:10.5194/acp-5-2099-2005, 2005.
- Tilstra, L. G. and Stammes, P.: Earth reflectance and polarization intercomparison between SCIAMACHY onboard Envisat and POLDER onboard ADEOS-2, *J. Geophys. Res.*, 112, D11304, doi:10.1029/2006JD007713, 2007.
- Tilstra, L. G., Schutgens, N. A. J., and Stammes, P.: Analytical calculation of Stokes parameters  $Q$  and  $U$  of atmospheric radiation, *Sci. Rep. WR 2003-01*, Koninklijk Ned. Meteorol. Inst., De Bilt, the Netherlands, available at: <http://www.knmi.nl/publications/fulltexts/wr200301.pdf> (last access: 4 July 2014), 2003.

- Tilstra, L. G., van Soest, G., and Stammes, P.: Method for in-flight satellite calibration in the ultraviolet using radiative transfer calculations, with application to Scanning Imaging Absorption Spectrometer for Atmospheric Chartography (SCIAMACHY), *J. Geophys. Res.*, 110, D18311, doi:10.1029/2005JD005853, 2005.
- van de Hulst, H. C.: *Light Scattering by Small Particles*, Dover Publications, Mineola, New York, 1981.
- Wang, P., Stammes, P., van der A, R., Pinardi, G., and van Roozendael, M.: FRESCO+: an improved O<sub>2</sub> A-band cloud retrieval algorithm for tropospheric trace gas retrievals, *Atmos. Chem. Phys.*, 8, 6565–6576, doi:10.5194/acp-8-6565-2008, 2008.